catalysts

MDPI

Article

Hydrogen-Ignited-Methanol Catalytic Co-Combustion of Aromatic Volatile Organic Compounds over PdPt/Al_2O_3 Bimetallic Catalyst

Sehrish Munsif [1,2], Lutf Ullah [1,2], Long Cao [1,2], Palle Ramana Murthy [1], Jing-Cai Zhang [1] and Wei-Zhen Li [1,2,*]

[1] CAS Key Laboratory of Science and Technology on Applied Catalysis, Dalian Institute of Chemical Physics, Chinese Academy of Sciences, Dalian 116023, China; sehrish@dicp.ac.cn (S.M.); lutfiktk77@dicp.ac.cn (L.U.); caolong@dicp.ac.cn (L.C.); ramanapalle@163.com (P.R.M.); zjc@dicp.ac.cn (J.-C.Z.)
[2] University of Chinese Academy of Sciences, Beijing 100049, China
* Correspondence: weizhenli@dicp.ac.cn

Abstract: Electric heating is frequently employed to treat volatile organic compounds (VOCs) through catalytic combustion. However, it is associated with problems such as slow heating, high energy consumption, and low efficiency. This study explores PdPt/Al_2O_3 catalysts for igniting methanol (MeOH) through H_2 catalytic combustion, providing internal on-site heating of catalyst active sites. It also investigates VOCs' abatement using H_2-ignited-MeOH combustion without H_2 and external heating. Bimetallic catalysts enhance activity and reduce thermal aging. Hydrogen gas (H_2) can initiate the MeOH combustion at room temperature with the addition of very small amounts, even below its low explosive limit of 4%. This process optimizes MeOH ignition at approximately 350 °C, even when the concentration of H_2 is as low as 0.01%. This method enhances combustion kinetics, converting MeOH and VOCs into CO_2 and water. Catalytic performance is independent of PdPt nanoparticle sizes in fresh and spent catalysts, represented in XRD and STEM. Using hydrogen as an igniting agent provides a clean, effective method to initiate catalytic reactions, addressing traditional challenges and enhancing VOCs' decomposition efficiency.

Keywords: PdPt/Al_2O_3 catalyst; aromatic VOCs; hydrogen-ignited-methanol catalytic combustion

Citation: Munsif, S.; Ullah, L.; Cao, L.; Murthy, P.R.; Zhang, J.-C.; Li, W.-Z. Hydrogen-Ignited-Methanol Catalytic Co-Combustion of Aromatic Volatile Organic Compounds over PdPt/Al_2O_3 Bimetallic Catalyst. *Catalysts* **2024**, *14*, 637. https://doi.org/10.3390/catal14090637

Academic Editor: Eric M. Gaigneaux

Received: 19 August 2024
Revised: 12 September 2024
Accepted: 14 September 2024
Published: 19 September 2024

1. Introduction

Atmospheric pollution from industrial and residential activities, particularly through volatile organic compounds (VOCs), poses significant risks to human health and the environment. VOCs, prevalent in industries like petrochemical, printing, and transportation, are key contributors to $PM_{2.5}$, ground-level ozone formation, photochemical smog, and ozone layer depletion [1]. Among VOCs, BTX (benzene, toluene, and xylene) is especially concerning due to its toxicity [2]. Various VOCs' removal strategies, including adsorption, condensation, and photocatalysis, have been explored. The complete oxidation of volatile organic compounds (VOCs) has been a significant focus for researchers, with a preference for supported noble metals. In different approaches, catalytic oxidation is considered the most efficient due to its high destruction rate and lower energy consumption, particularly at temperatures 300–600 °C, especially for low VOCs' concentrations [3–6].

Noble-metal catalysts are highly effective for VOCs' oxidation due to their superior activity and selectivity, making them ideal for low-temperature complete oxidation. However, due to challenges such as high cost, limited availability, uneven geographical distribution, and susceptibility to self-poisoning, attention has increasingly turned toward catalysts based on transition metals. Commonly used catalyst supports for noble metals include metal oxides like Al_2O_3, ZrO_2, CeO_2, and SiO_2 [3,7–10]. Aluminum oxide (Al_2O_3) is widely used due to its amphoteric properties, allowing it to act as both an acid and a base, depending on the medium. Its high melting point and polymorphism enhance its role in stabilizing

fine catalyst particles, preventing agglomeration. The γ-Al_2O_3 phase is particularly active and commonly employed in catalysis because of its high surface area (100–400 m^2/g), thermal stability, and favorable surface properties, such as acid–base behavior [11–13].

Several key variables, including the structure and concentration of VOCs and temperature, influence the breakdown of VOCs. Higher temperatures can expedite the abatement process [14]. Among these, noble metals such as Pd and Pt, supported by γ-Al_2O_3, have been extensively utilized due to their high activity in oxidation reactions despite their higher costs [15,16]. While Pt and Pd, individually or as bimetallic catalysts, have been extensively studied, Pd exhibits superior thermal and hydrothermal sintering resistance compared to Pt, enhancing both catalytic activity and stability [17]. Pd catalysts are deactivated more readily when used alone, and thus, Pt is commonly combined with Pd to enhance their durability and tolerance to sulfur and H_2O. Bimetallic-supported catalysts generally outperform single-component catalysts and showcase activity that varies based on composition [18]. A recent study found that a bimetallic Pd–Pt catalyst outperformed a monometallic Pd catalyst, showing better activity and durability, especially during methane combustion [17,19]. Hence, energy consumption remains a major concern, prompting researchers to optimize this technology for lower energy usage and cost-effectiveness [20].

In particular, hydrogen significantly reduces ignition temperatures. Experiments at low hydrogen mole fractions (1.5%) reveal its positive chemical impact on catalytic ignition, leveraging the self-ignition reaction of hydrogen gas on catalyst surfaces like Pt for fuel ignition. Higher H_2 concentrations, however, raise the ignition temperature, emphasizing the thermal effect of H_2 [21]. This study investigates how hydrogen assists in igniting n-butane on platinum in a small combustion setup. A critical amount of hydrogen (3.1% at an equivalence ratio of 0.8 and 1.7% at 0.4) was found to be crucial, marking the threshold between these effects. Interestingly, even a small amount of hydrogen was sufficient for catalytic ignition, enabling ignition at room temperature without specialized equipment [22]. Besides some limitations, methanol is an excellent alternative fuel with a high energy conversion efficiency. It may also be produced through several renewable energy sources; the most effective form of carbon capture is recycling CO_2 to produce methanol [23].

Methanol is a great fuel for spark-ignition engines since it has a lot of favorable qualities, such as the high heat of vaporization, also known as "latent heat", low stoichiometric air–fuel ratio (AFR), high specific energy ratio (i.e., energy per unit of fuel–air mixture), a rapid flame speed, rich molar expansion ratio, minimal combustion temperature, excessive hydrogen-to-carbon ratio, and a liquid at standard temperature and pressure (STP). These are just some of its favorable qualities; also, a notable quality of methanol is that it burns very cleanly, as shown when it was previously employed as a fuel for air quality purposes [24]. This investigation delves into the intricate interactions between the bimetallic catalyst, hydrogen ignition, and methanol combustion. By rebooting the catalytic system, the aim is to achieve superior catalytic efficiency, leading to enhanced VOCs removal and reduced environmental impact. The comparison between hydrogen and methanol highlights key considerations for each fuel. The hydrogen-ignited catalytic methanol combustion is an efficient and environmentally friendly method of treating VOCs.

In this work, we explored the catalytic combustion of benzene, toluene, ethylbenzene, and xylene (BTEX) using a $PdPt/Al_2O_3$ catalyst, where hydrogen-ignited-methanol initiates the complete oxidation of these aromatic VOCs. In addition to rapid temperature increases, minimal pollution, and economic feasibility, reactions occur at room temperature. The spent $PdPt/Al_2O_3$ catalyst continuously retains its ignition capability for hydrogen-ignited-methanol combustion at room temperature. This study examines novel VOCs' abatement methods, evaluating how varying VOCs, 0.01% methanol, and 3% H_2 concentrations impact catalytic combustion and comparing energy consumption between traditional electric heating and hydrogen-ignited-methanol combustion.

2. Results

2.1. Structure Evolution of PdPt/Al_2O_3 Catalyst

2.1.1. X-ray Diffraction

The XRD patterns of the alumina and fresh and spent Pd/Al_2O_3 and PdPt/Al_2O_3 catalysts are depicted in Figure 1, respectively. The characteristic diffraction peaks of γ-Al_2O_3 (gamma-alumina) were observed at 2θ angles of 19.5°, 32.9°, 37.5°, 39.5°, 45.7°, 60.7°, and 67.0°. Initially, only characteristic Al_2O_3 diffraction peaks were observed in the Pd/Al_2O_3-fresh obtained sample, with no discernible peaks attributable to Pd, indicating an initially uniform distribution of Pd on the Al_2O_3 support. However, for the spent monometallic Pd/Al_2O_3 catalyst at 2θ = 33.8° and 54.7°, two additional peaks emerged, corresponding to the (101) and (112) planes of PdO, respectively (JCPDF = 85-0713) [19,25,26]. The XRD analysis of bimetallic PdPt catalyst revealed diffraction peaks corresponding to Pt, Pd, cubic fluorite-type oxide, and Al_2O_3, indicating the successful formation of the desired catalysts without any crystalline impurities. Nevertheless, metallic Pt originates from the prominent distinctive diffraction peaks at 2 theta angles of 39.8°, 46.3°, 67.5°, 81.3°, and 85.8° (JCPDF-04-0802). The PdPt/Al_2O_3-fresh catalyst did not exhibit the distinctive diffraction peaks of Pd, Pt, or PtOx species, suggesting that these species are either extremely scattered or amorphous in these catalysts. The bimetallic PdPt/Al_2O_3-spent catalyst's XRD patterns exhibited minor diffraction peaks at 2θ values of 60.9° peak, associated with the PdO (200) planes. The hydroxyl groups may have adhered to the catalyst's surface and caused the PdO peaks to appear in the spent catalyst. Since the catalyst was cooled in the air after the reaction tests were stopped at a high temperature, PdO rather than metallic Pd was expected to form. Additionally, there was a prominent Pt (111) plane observed at an angle of 39.8°, which was likely due to aggregation. This results can also be observed in below Figure 5b as well.

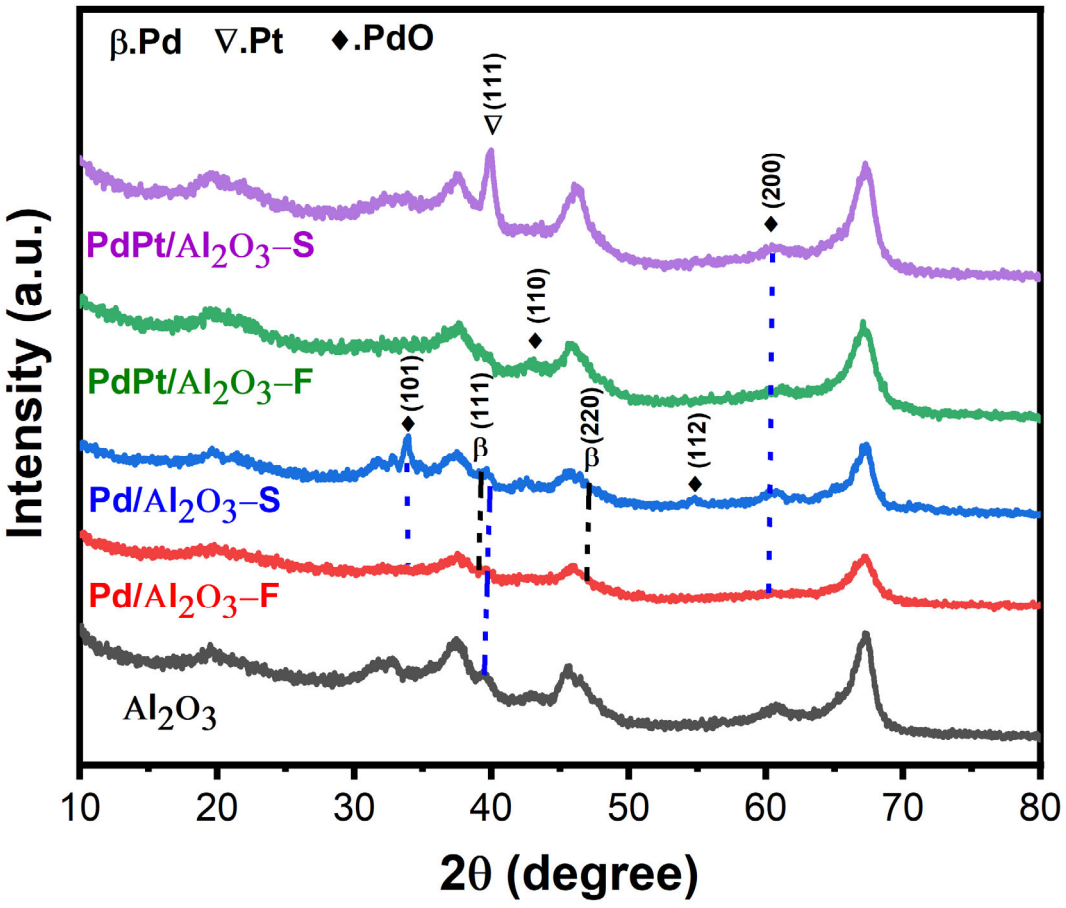

Figure 1. XRD patterns for alumina and fresh (F) and spent (S) Pd/Al_2O_3 and PdPt/Al_2O_3 catalysts.

The presence of metallic palladium (characteristic peak at 40.1°) is unlikely because palladium typically oxidizes after calcination in air. Generally, the lattice constant of PdPt is smaller than that of Pt (3.924 Å) but larger than that of Pd (3.891 Å). Therefore, when the bimetallic is formed, a shift in the Pt peak to higher diffraction angles is expected [3,27–30].

2.1.2. BET Analysis

The physicochemical properties of bare alumina and mono-metallic and bimetallic catalysts are explained in Table 1. Before the analysis, the samples were pretreated to remove the impurities stuck inside the sample's pores. The incorporation of Pd and PdPt onto the Al_2O_3 support significantly influenced its textural properties. The surface area of the bare alumina (115.9 m^2/g) increased upon metal loading, with fresh $PdPt/Al_2O_3$ catalyst exhibiting the highest surface area (251.3 m^2/g). The increase in surface area was attributed to the dispersion of metal nanoparticles across the alumina surface, which prevented pore blockage and maintains accessibility to internal surfaces. As shown in Table 1, the fresh bimetallic catalyst surface area was higher than that of the monometallic catalysts due to the interaction between the two metals [31]. However, we observed opposite results in the spent catalysts, presumably due to the aggregation of Pt, which can block the pore of the support.

Table 1. Physicochemical characteristics of the Al_2O_3, Pd/Al_2O_3-F & S, and $PdPt/Al_2O_3$-F & S samples.

Sample	S_{BET} (m^2/g)	Pore Size (nm)	Pore Volume (cm^3/g)
Al_2O_3	115.9	4.9	2.7
Pd/Al_2O_3-F *	208.1	6.6	0.4
Pd/Al_2O_3-S #	164.8	8.4	0.4
$PdPt/Al_2O_3$-F	251.3	6.3	0.5
$PdPt/Al_2O_3$-S	143.3	8.8	0.4

* F = Fresh and # S = Spent.

Additionally, the pore size of the catalysts increased upon metal incorporation, with spent Pd/Al_2O_3 and $PdPt/Al_2O_3$ showing larger pore diameters (8.4 nm and 8.8 nm, respectively) compared to the bare Al_2O_3 (4.9 nm). This suggests that metal particles may restructure the alumina support, enlarging the pores. However, the pore volume decreased, likely due to partial blockage by metal nanoparticles and/or compaction of the support. Fresh mono and bimetallic catalysts surface areas were higher than their spent counterparts. These results showed that the catalysts' surface area decreased after being used several times at higher temperatures on a longer term. However, a decrease in surface area did not affect the VOCs' oxidation. Among all, fresh $PdPt/Al_2O_3$ had a higher surface area and pore volume than other catalysts, and the pore size was higher for the spent catalysts than the fresh catalysts.

The N_2 adsorption–desorption isotherms and pore size distribution curves for alumina (Al_2O_3), as well as fresh and spent catalysts (Pd/Al_2O_3 and $PdPt/Al_2O_3$), are depicted in Figure 2, with the corresponding parameters detailed in Table 1. The presence of hysteresis loops at P/P_0 = 0.6−1.0 confirmed the mesoporous nature of the catalysts, and all isotherms were classified as type IV [32]. Figure 2c,d clearly show that the addition of noble metals had minimal impact on the type of hysteresis loop and pore size distribution of the samples. However, as indicated in Table 1, it did influence their surface areas and total pore volumes [33].

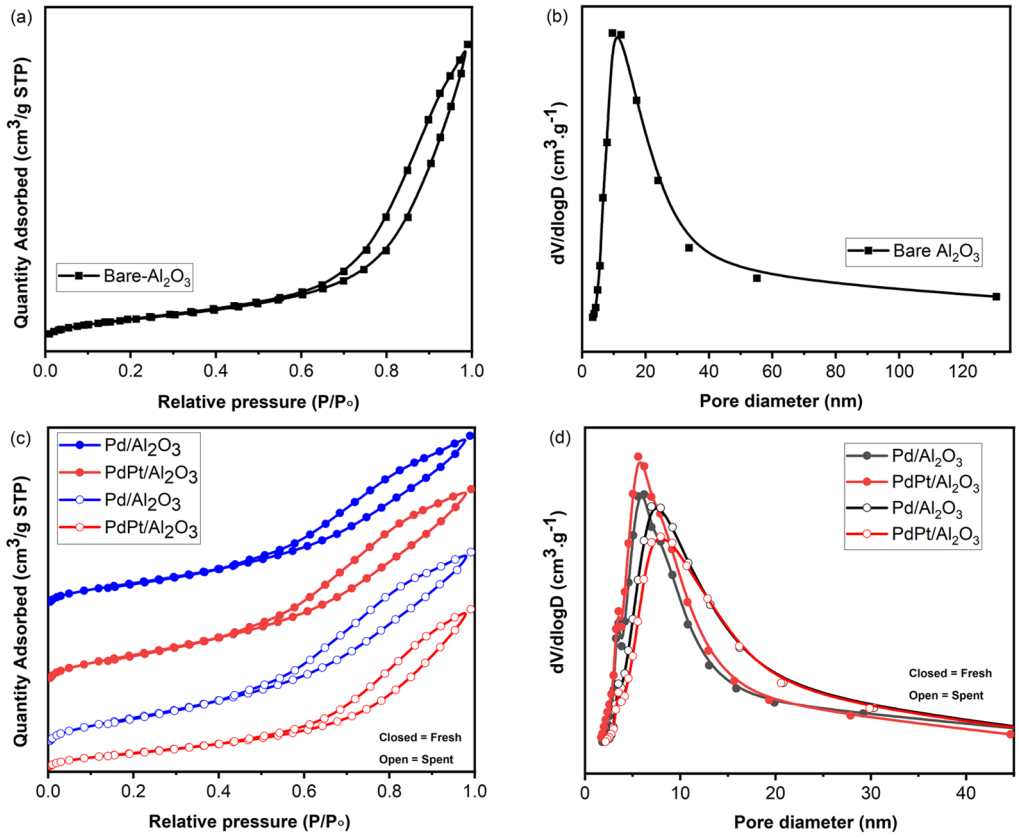

Figure 2. The N_2-sorption isotherms and pore size distribution of (**a**,**b**) alumina supports and (**c**,**d**) fresh and spent (Pd/Al_2O_3 & $PdPt/Al_2O_3$) catalysts.

2.1.3. STEM Analysis

The initial dispersion and structural changes of Pd and Pt were investigated using STEM images (Figure 3), HAADF imaging, and element mapping (Figure 4). In the fresh $PdPt/Al_2O_3$ sample (Figure 4a), numerous small Pd and Pt nanoparticles (2–5 nm) were observed, highlighted by yellow circles, indicating high dispersion over the Al_2O_3 support. The bare alumina exhibited a porous surface structure with predominantly spherical particles averaging 50 nm in diameter, shown in Figure S1.

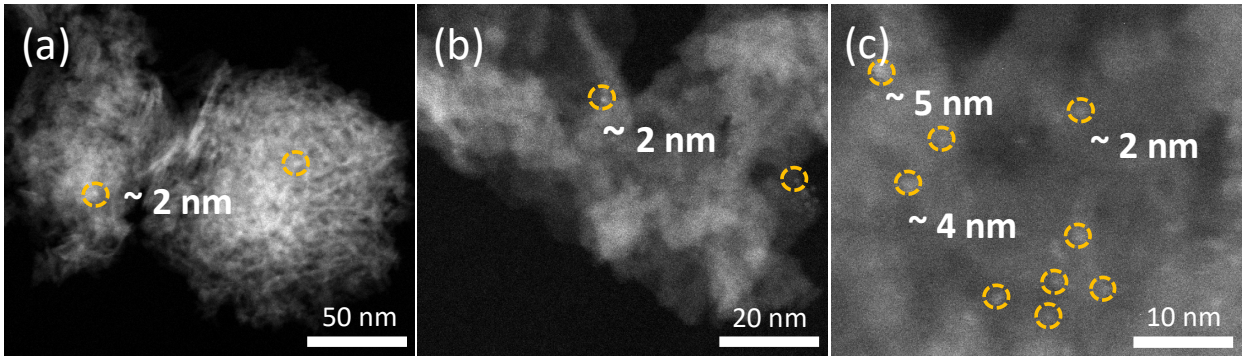

Figure 3. Displays STEM images (**a**–**c**) of the fresh $PdPt/Al_2O_3$ catalyst.

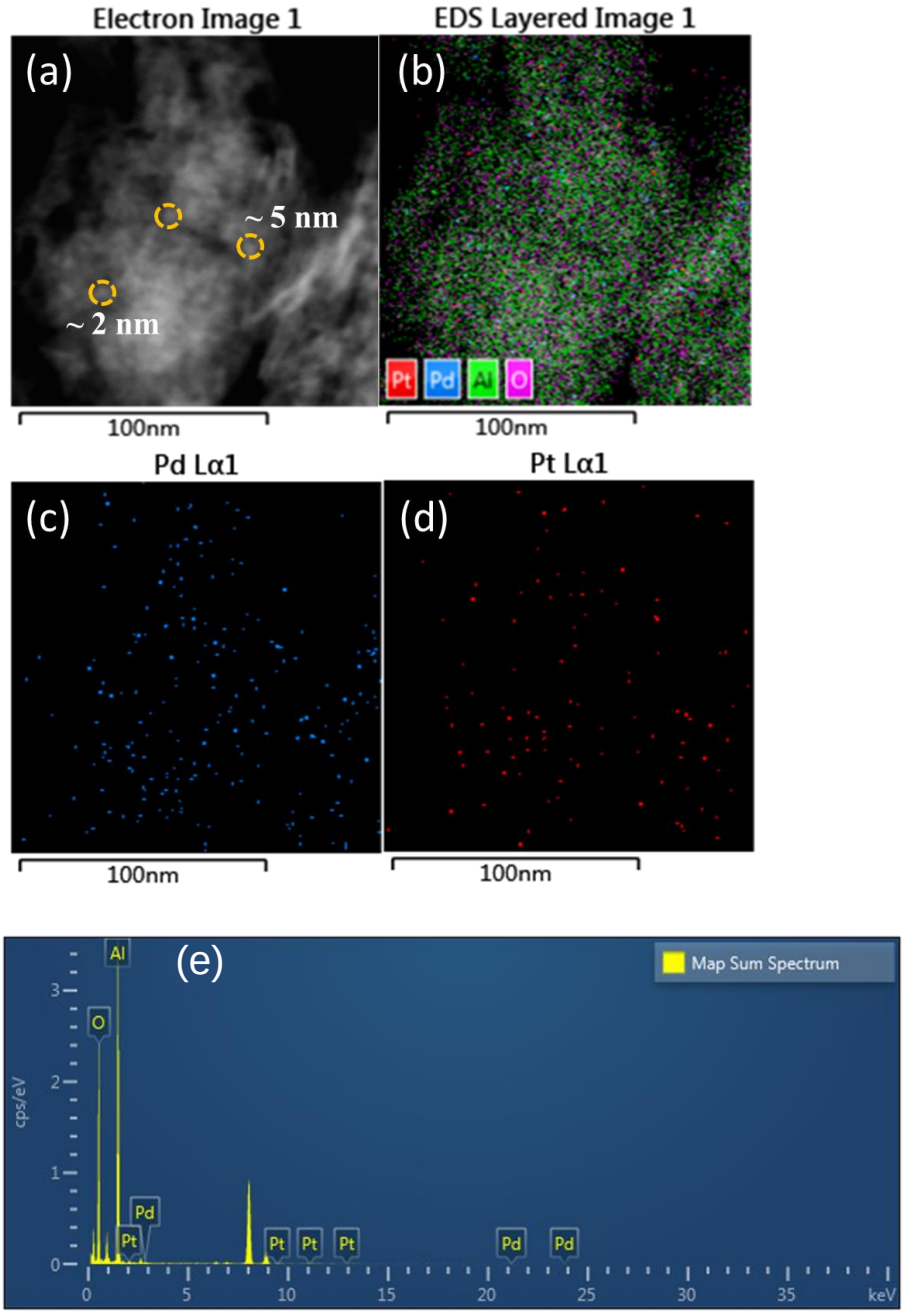

Figure 4. HAADF image (**a**) element mapping images (**b**–**d**) and EDX spectrum (**e**) for fresh $PdPt/Al_2O_3$ catalyst.

The element mapping (Figure 4b–d) further confirmed the presence of smaller Pd species represented by scattered blue (Pd) and red (Pt) dots [34]. In contrast, the spent $PdPt/Al_2O_3$ catalyst (Figures 5 and 6a) showed very few Pd particles [18] but large Pt particles (10–41 nm) with sparse red aggregations in the element mapping (Figure 6b–d). It suggests that the sintering of Pt nanoparticles occurred, leading to the agglomeration of Pt particles, a phenomenon commonly reported in the literature for conventional $PdPt/Al_2O_3$ catalysts. The presence of these elements was further confirmed by the EDX spectra shown in Figures 4e and 6e.

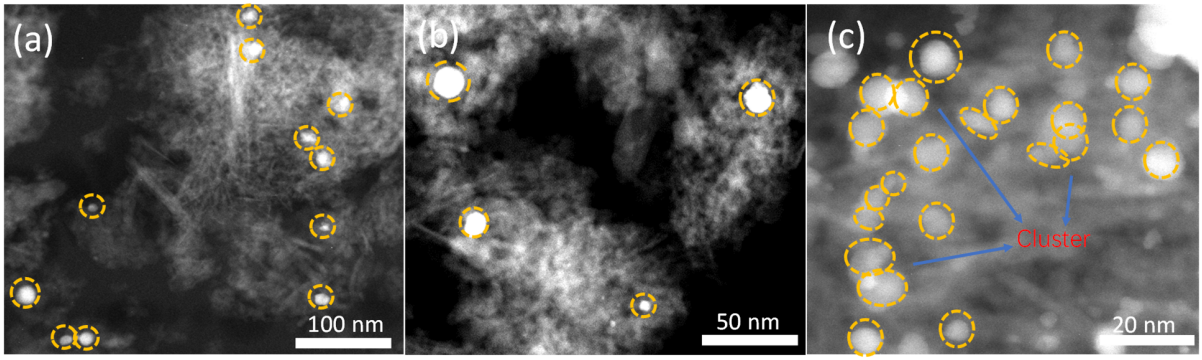

Figure 5. Displays STEM images (**a**–**c**) of the spent $PdPt/Al_2O_3$ catalyst.

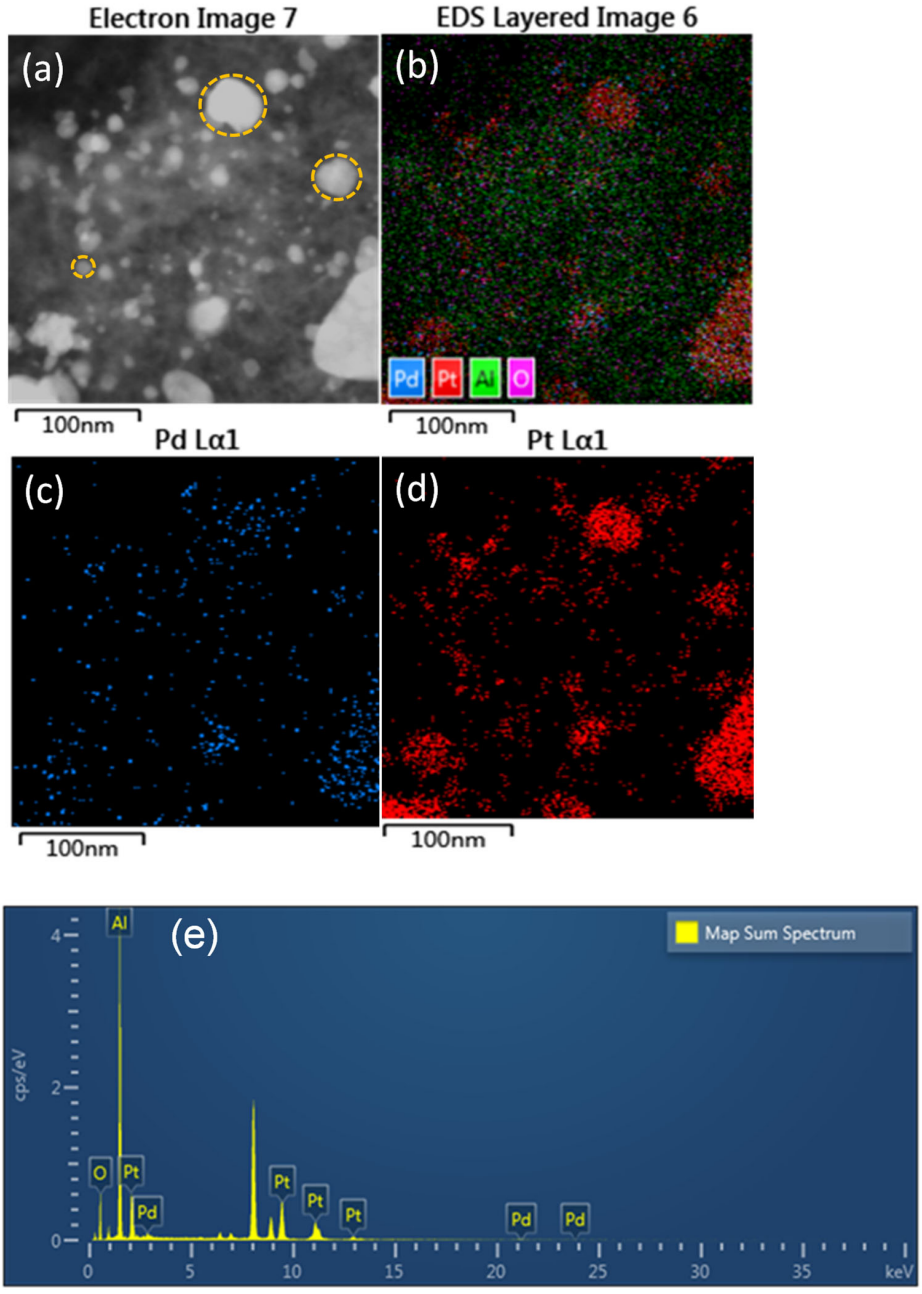

Figure 6. HAADF image (**a**) and element mapping images (**b**–**d**), EDX spectrum (**e**) for spent $PdPt/Al_2O_3$ catalyst.

2.1.4. ICP Analysis

The ICP analysis revealed that the fresh $PdPt/Al_2O_3$ catalyst contained 0.6 wt.% Pd and 1.1 wt.% Pt. After the catalytic tests, the spent catalyst exhibited a slight decrease in metal content, with 0.5 wt.% Pd and 1.0 wt.% Pt, indicating minimal leaching of the active metals during the reaction.

2.2. Catalytic Performance Assessment

The $PdPt/Al_2O_3$ catalyst was employed for the catalytic oxidation of H_2, methanol, and VOCs. Initially, we determined the light-off temperatures for various VOCs over the fresh $PdPt/Al_2O_3$ catalyst using temperature-programmed reactions on an electric heating furnace. Figure 7 illustrates the light-off curves of CO_2 formation and the corresponding catalyst bed temperature profiles. For benzene, a significant increase in the CO_2 signal occurred on a stream of 33 min, with the temperature exceeding 900 °C. The CO_2 signal exhibited a peak from 34 to 41 min, with temperatures surpassing those following the ramping slope, indicating the exothermic nature of benzene combustion. Upon further increasing the furnace temperature, the CO_2 signal plateaued above 900 °C, signifying the complete oxidation of benzene.

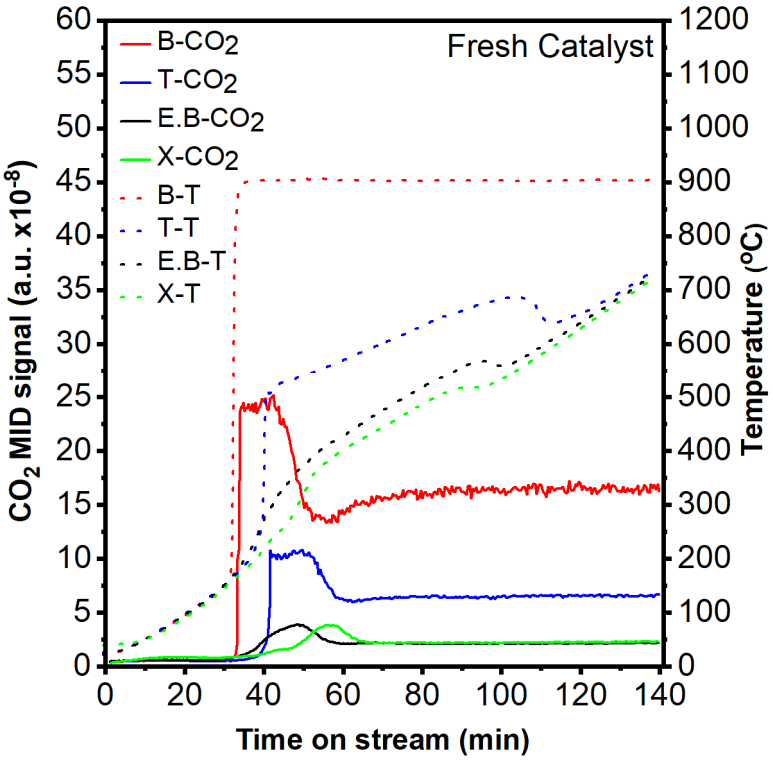

Figure 7. Light-off curves illustrated by CO_2 formation and catalyst bed temperature raising profiles during the temperature-programed reaction of benzene (B), toluene (T), ethyl benzene (E.B), and xylene (X) over 0.5 g fresh $PdPt/Al_2O_3$ catalyst using the electric heating furnace. The VOCs' concentrations were controlled at 10% vapor, and the temperature ramping rate was 5 °C/min.

To ensure safety, the furnace temperature was stabilized at 200 °C. For toluene, the CO_2 signal also increased from 42 min to 50 min, and the corresponding temperature increased to 506 °C. There is also an exothermic effect and a lower temperature compared to benzene, possibly due to less vapor pressure and low heat of combustion (~−3910 kj/mol) as mentioned in Table 2. In this case, the temperature increased from 42 min to 106 min, from 506 °C to 687 °C, then fell to 641 °C, and then increased slowly. Along with the above-mentioned results of benzene, intense CO_2 peaks were observed between 23.2 and 26.2 min, followed by a gradual decrease to a stable level. This behavior was attributed to previously adsorbed benzene on the catalyst surface, which was released due to slow

electric heating and its high vapor pressure. Once benzene reached its light-off temperature and conversion began after 41 min, the T-CO_2 signal decreased because the absorbed VOCs, particularly benzene, were likely mostly consumed. With available benzene for combustion, CO_2 production decreased and then stabilized. A similar effect was observed for toluene, with CO_2 peaks occurring between 34 and 41 min.

Table 2. Vapor pressures and heat of combustion for various VOCs, and the nominal concentrations and calorific values for mixtures of VOCs and air in different compositions.

Chemical	Vapor Pressure (20 °C, kPa)	Heat of Combustion (25 °C, kJ/mol)	Nominal Concentration (%)			Calorific Value (kJ/m^3)		
			10% Vapor	20% Vapor	30% Vapor	10% Vapor	20% Vapor	30% Vapor
Hydrogen	**--**	286	--	--	--	--	--	--
Methanol	13.0	725	1.3	2.6	3.9	420.8	841.5	1262.3
Benzene	10	3263	0.99	1.98	2.97	−1435.72	−2884.25	−4326.27
Toluene	9	3910	0.29	0.58	0.87	−504.39	−1012.48	−1517.19
[a] E. benzene	1.33	4568	0.13	0.26	0.39	−269.12	−530.21	−795.32
Xylene	1.33	4568	0.13	0.26	0.39	−269.12	−530.21	−795.32

[a] Ethyl benzene = E. benzene.

In the ethyl benzene case, a very low CO_2 peak covered from 34 min to 50 min and a temperature peak from 254 °C to 568 °C. Then the temperature decreased to 559 °C, but it later started increasing. In the case of xylene, a similar temperature behavior to that of ethyl benzene was observed due to the same vapor pressure and heat of combustion, as shown in Table 2. In this case, temperature increases ranged from 357 °C to 510 °C during 54 min to 87 min. However, the CO_2 signal appeared a little later than ethyl benzene, from 40 to 57 min. In short, the light-off temperatures for benzene, toluene, ethyl benzene, and xylene were 160 °C, 220 °C, 215 °C, and 270 °C, respectively.

The heating efficiency of the catalytic combustion of methanol in 3%H_2 over Pd/Al_2O_3 and $PdPt/Al_2O_3$ catalysts was evaluated by varying the methanol concentrations under GHSV of 120,000 mL/(g-h). As shown in Figure 8, the catalyst bed temperature jumped from 20 °C to ~230 °C once 3% H_2 was introduced, and it could remain stable with flowing H_2. It could reach and be maintained at ~350 °C when the +10 MeOH concentration was introduced over $PdPt/Al_2O_3$ (bimetallic catalyst), while for Pd/Al_2O_3, the temperature started decreasing and reached stability at room temperature. Further elevating the +20 MeOH concentration, the bimetallic catalyst could keep the temperature at ~400 °C. Further, increasing the MeOH concentration to +30, the catalyst bed temperature increased and was kept constant at ~435 °C. Notably, the catalyst bed could be heated to temperatures higher than light-off for benzene, toluene, ethyl benzene and xylene with +10 MeOH concentrations, over bimetallic catalyst. This catalyst showed great potential as a heating source to substitute electronic heating. On the other hand, monometallic become deactivated with each rise of methanol concentration, still at room temperature.

The catalytic efficacy of hydrogen-ignited-methanol in VOCs' purification rapidly elevated the catalyst bed temperature to reach the ignition temperature of VOCs within a brief duration, enabling VOCs' combustion at room temperature. Figure 9 illustrates the catalytic conversion of varied concentrations of aromatic VOCs in the presence of methanol used as fuel; specifically, the goal was to find the minimal hydrogen concentration required to ignite the methanol and also to identify the minimum methanol concentrations necessary for the full conversion of benzene, toluene, ethyl benzene and xylene. The reaction unfolded in six distinct steps, each lasting approximately 30 min. The initial phase introduced only air for 30 min to establish a steady baseline. In the subsequent step, 3% hydrogen gas permeated the system to attain a stable bed temperature.

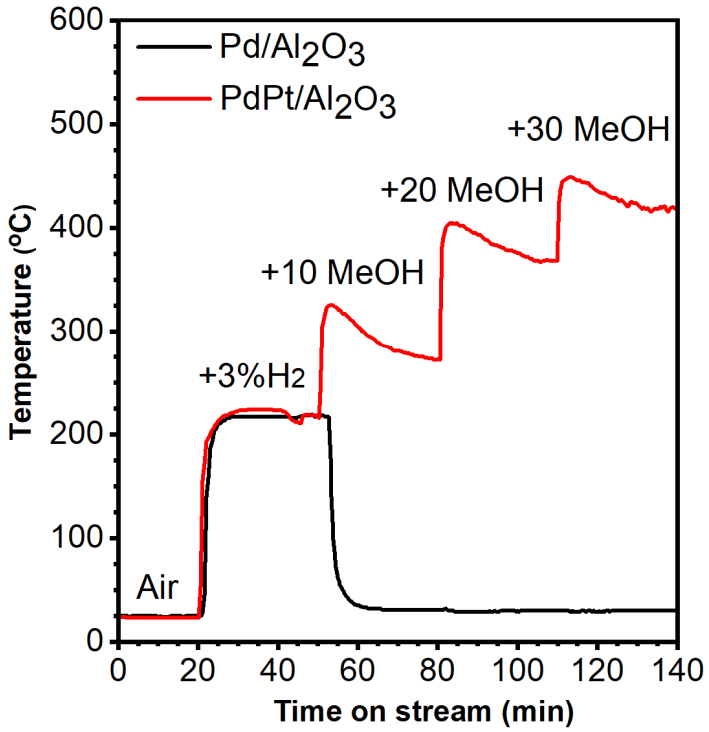

Figure 8. Temperatures of catalyst bed for +10 MeOH, +20 MeOH, and +30 MeOH ignited with 3% of H_2 in air with a total flow of 1000 mL/min over 0.5 g of $PdPt/Al_2O_3$ catalyst (GHSV: 120,000 mL/(h·g)).

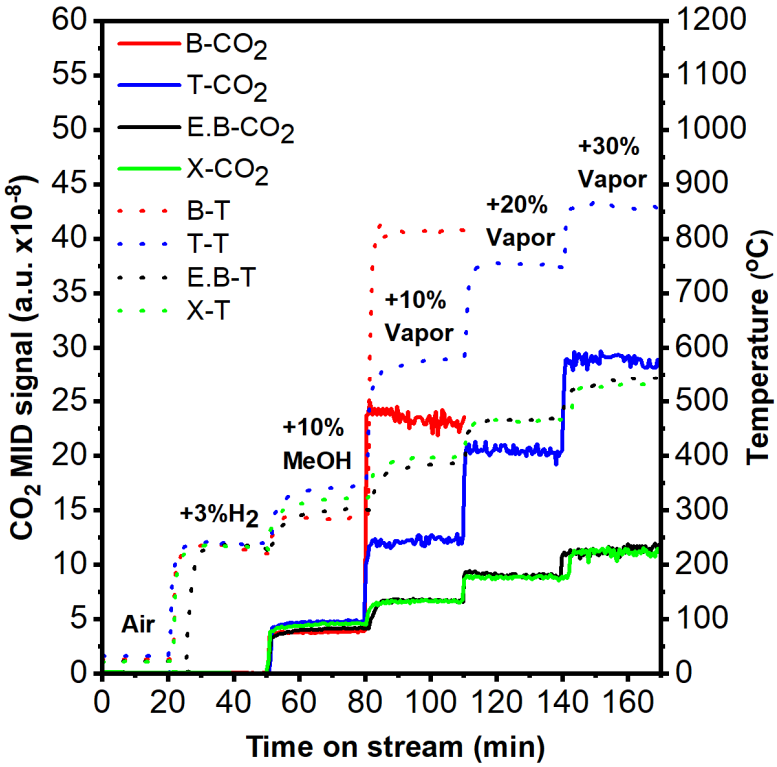

Figure 9. The curves of benzene (B), toluene (T), ethyl-benzene (E.B), and xylene (X) CO_2 formation and the corresponding catalyst bed temperature (T) profiles of various VOCs with co-combustion of MeOH started with 3%H_2 ignition over 0.5 g $PdPt/Al_2O_3$ catalyst.

Notably, the catalytic bed temperatures for the bimetallic catalyst ($PdPt/Al_2O_3$) were measured at 240 °C, after 60 min. Once a stable temperature was achieved, the subsequent reaction steps stopped hydrogen and introduced methanol. In the case of benzene, the introduction of 0.01% methanol concentrations induced a catalytic bed temperature exceeding 284 °C, again attaining a stable bed temperature. The rapid emergence of a CO_2 peak and the absence of a methanol peak indicated complete methanol conversion. Then 0.05% benzene was introduced, elevating the temperature to around 814 °C within a short duration; the appearance of an enhanced and prominent CO_2 peak and no benzene peak eventually led to complete conversion (Figure 9). This high temperature, which was challenging to manage, caused the catalytic bed to become red-hot, prompting the cessation of further reactions to ensure safety. During toluene combustion, the catalyst bed with methanol was 341 °C; no methanol peak was observed after diverse concentration of toluene were gradually introduced. In the subsequent four steps, the addition of 0.018% toluene resulted in the catalyst bed temperature rising to 579 °C with no toluene peak and a higher CO_2 peak (Figure 9), leading to complete combustion. With subsequent increases in toluene concentration to 0.036% and 0.054%, the bed temperature surged above 754 °C and 866 °C within a few seconds, respectively. In both steps, no toluene peak was observed, and higher CO_2 peaks originated (Figure 9), indicating the complete conversion of toluene.

Conversely, in ethyl benzene combustion, using a catalyst bed temperature with methanol 301 °C, there was no methanol peak as shown in Figure 9. Various injections of ethyl benzene, such as 0.0008%, 0.001%, and 0.002%, propelled the catalytic bed temperature beyond 379 °C, 464 °C, and 540 °C in the initial seconds, respectively. The absence of an ethyl benzene peak and increased CO_2 indicated the reaction was complete, while in xylene catalytic combustion, the bed temperature with MeOH was around 319 °C. This temperature was sufficient for total methanol conversion, as illustrated in Figure 9. Upon introducing 0.0001% xylene, resulting in the generation of carbon dioxide (CO_2), the bed temperature also increased to 395 °C, while with the other concentrations, the bed temperature was the same as ethyl benzene in Figure 9. In an overarching perspective, the presented reaction elucidates the correlation between methanol concentrations and the impact of various VOCs' concentrations on reaction temperatures during the catalytic conversion process. The nominal concentrations and calorific values for mixtures of VOCs and air in different compositions are given in Table 2 above.

2.3. Performance of Spent Catalyst

During the above catalyst performance assessments, the $PdPt/Al_2O_3$ catalyst suffered high temperatures of 900 °C in an oxygen-rich atmosphere. Hence, the spent catalyst had a sintering characteristic such as a decrease in surface area and aggregation of Pd, Pt, and Al_2O_3 nanoparticles (Figures 1, 5 and 6). The catalytic performance of the spent catalyst was evaluated by the light-off temperatures for various VOCs using temperature-programmed reactions on an electric heating furnace. As shown in Figure 10, a steep CO_2 rise was observed at 34 min to 41 min for the fresh catalyst, while in the spent catalyst, it was observed at 38 min to 50 min where the light-off temperature was 168 °C for benzene over the spent $PdPt/Al_2O_3$ catalyst. The temperature was decreased from 900 °C over the fresh catalyst to 850 °C. For toluene, a CO_2 peak was observed at 46 min to 55 min, a little far from the peak observed over the fresh catalyst.

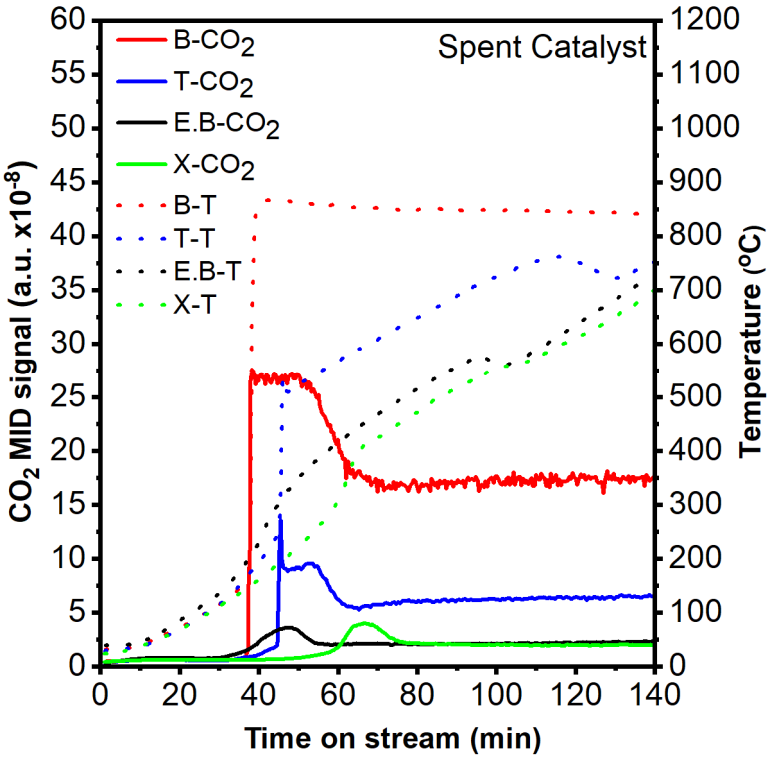

Figure 10. Light-off curves illustrated by CO_2 formation and catalyst bed temperature raising profiles during temperature-programed reaction of benzene, toluene, ethyl benzene, and xylene over 0.5 g spent $PdPt/Al_2O_3$ catalyst using an electric heating furnace. The VOCs' concentrations were controlled at 10% vapor, and the temperature ramping rate was 5 °C/min.

For ethyl benzene and xylene, a similar shifting of peaks was noticed over spent compared to fresh catalysts. These results indicate that the spent catalyst was still highly active for catalyzing VOCs' oxidation, in line with the facts that there was no detectable deactivation during the above H_2, methanol, and VOCs' co-feeding tests. In the bimetallic spent catalyst, only a few Pt nanoparticles exhibited aggregation, while the Pd nanoparticles remained unchanged and effective, as confirmed by element mapping in Figure 5. The use of spherical Al_2O_3 support, compared to an amorphous one, resulted in more uniform heating. This spherical shape promoted hotspot heating, which minimizes the effects of particle sintering or accumulation. Consequently, it retains a high number of active nanoparticles, ensuring consistent catalytic activity even in the spent catalyst. In contrast, amorphous supports may lead to a more substantial loss of activity.

2.4. Hydrogen-Ignited-Methanol Effect

To investigate the impact of hydrogen-ignited-methanol on the catalytic combustion of VOCs, the experiment was conducted in the presence and absence of hydrogen-ignited-methanol, involving six distinct steps. Before introducing VOCs, air was passed through the system to cleanse the path and prevent contamination. After a 30-min interval, a stable baseline with air was established. Subsequently, a small amount of +10 vapor of VOCs was introduced, resulting in no observed CO_2 peak or temperature rise even after an additional 30 min, as shown in Figure 11. However, clear and enhanced VOCs (benzene, toluene, ethyl benzene, and toluene) peaks were noticed in Figure S2, Supplementary Information.

An optimal hydrogen concentration and minimum methanol concentration were selected to elucidate the role of hydrogen-ignited-methanol in VOCs' conversion. Turning off VOCs and introducing 3% hydrogen resulted in a bed temperature reaching 240 °C for all the VOCs as given in Figure 11, Figures S2 and S3 (Supplementary Information).

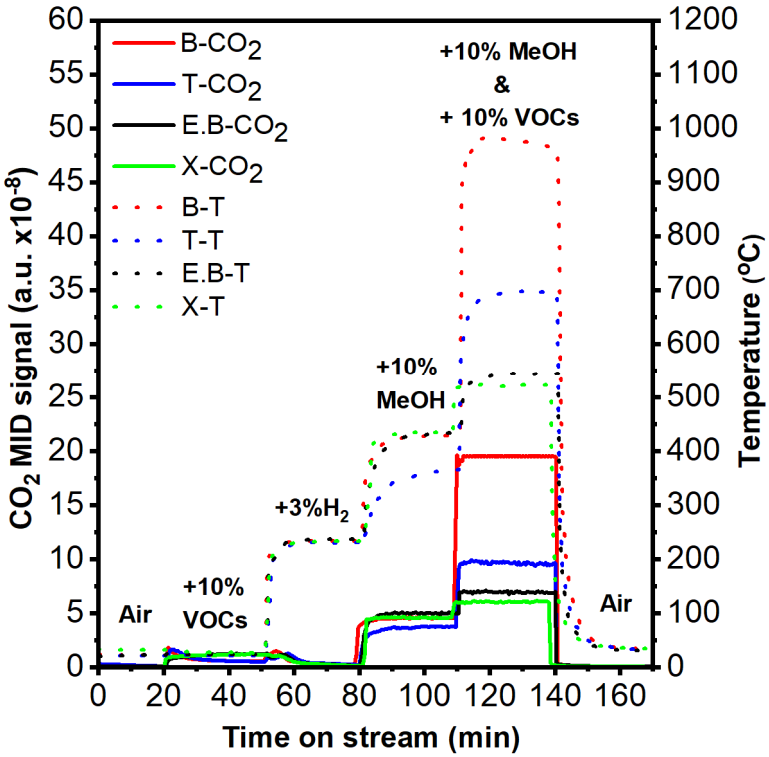

Figure 11. CO_2 formation curves and the corresponding catalyst bed temperature profiles of various VOCs with co-combustion of +10 MeOH started with 3%H_2 ignition over 0.5 g PdPt/Al_2O_3 catalyst.

In the next step, turning off hydrogen and introducing 0.01% MeOH into the system led to a noticeable increase in temperature, accompanied by the emergence of a CO_2 peak shown in Figure 11. At the same time, the methanol peak disappeared, as shown in Figure S3. As the temperature gradually rose, so did the CO_2 conversion. Upon reaching the maximum temperature, complete methanol conversion was achieved. Different VOCs had different bed temperatures in this step. For example, benzene, ethyl benzene, and xylene had bed temperatures of ~440 °C, and toluene had a bed temperature of 350 °C. The reaction was initiated with +10 vapors of each VOC (benzene, toluene, ethyl benzene, and xylene), causing a significant rise in bed temperature to 982 °C, 697 °C, 544 °C, and 520 °C, respectively. As temperature increased, VOCs' combustion began, generating CO_2 without a VOCs peak, resulting in complete VOCs' conversion as shown in Figures 11, S2 and S3 (Supplementary Information). Then methanol and VOCs supplies were halted, and air was reintroduced. The CO_2 and temperature peaks gradually decreased, eventually stabilizing at the same level as in the initial step, as shown in Figures 11, S2 and S3.

The experimental findings demonstrate that adding hydrogen increases the bed temperature and activates the methanol combustion, allowing the appearance of the CO_2 peak along with a temperature increase of around 450 °C over time. This temperature is sufficient for methanol to facilitate the VOCs' combustion and confirm the occurrence of complete combustion at this elevated temperature.

3. Discussion

3.1. Heating Technology Comparison: Electric vs. Co-Combustion

In the traditional method, VOCs' combustion is performed in a fixed-bed reactor inside a resistance furnace. This furnace operates on the Joule heating principle, generating heat through resistors on the chamber walls. The electrical energy transforms into heat, raising the reactor's temperature. However, some heat is lost to the furnace walls, reducing efficiency. This method used radiation and conduction to start the reaction between the reactant gases and the catalyst that was located inside the reactor, utilizing an external high

furnace temperature. Due to its highly exothermic nature, hydrogen ignites in air without releasing heat, achieving an adiabatic flame temperature of 2127 °C [35,36]. For onsite heating via H_2 combustion, most of the hydrogen's chemical energy was effectively utilized to elevate the temperature of the catalytically active PdPt sites to the system's maximum. Since the reactor and furnace do not need to be heated in total, co-combustion heating is far more energy-efficient than electric furnace heating [37].

3.2. Catalytic Advantages of Onsite Heating with H_2-Ignited Methanol Combustion

A macroscopic-scale evaluation revealed that the catalytically active PdPt sites were substantially heated to the system's maximum temperature by utilizing the chemical energy of H_2. When heated through flowing H_2, this temperature was high enough to start the reaction in the catalyst bed. However, the reaction heat was transferred from the PdPt sites to other locations, with the PdPt sites where the H_2 catalytic combustion occurred becoming the hottest regions [36,38]. Additionally, co-fed VOCs can also contribute to the catalytic combustion process. For instance, in previous work, the bed temperature reached 450 °C when a gaseous reactant mixture, such as air and 2% H_2, was added along with 10% methanol vapors.

Considering methanol as an example, the exchange heat of hot air and water can be used to heat the methanol molecule before it comes into contact with hot PdPt sites. Changing the quantities of H_2 and methanol makes it easy to modify the temperature of the PdPt and methanol sites. According to earlier research, a considerable temperature differential is produced when the amount of methanol vapor in a catalyst bed containing hydrogen is increased. The top third of the bed heats up to 695 °C with 20% methanol vapor, 2% hydrogen, and air flow. The temperature in the upper half of the bed rises to 865 °C when methanol is increased to 30%. This suggests that the upper part of the catalyst bed is where the exothermic combustion event is completed [37].

Using methanol as a fuel, apart from the points discussed in the introduction section, two key characteristics of methanol are noteworthy. First, methanol can burn extremely cleanly; it has been used to improve air quality. With only a single carbon atom, it does not easily form carbonaceous particulate matter like long-chain hydrocarbons, similar to methane. Second, methanol is the simplest carbon-based molecule that is liquid at standard temperature and pressure (STP), making it easy to store and transport with minimal losses in both vehicles and fuel infrastructure.

The total bed temperature can reveal the impacts even while the precise temperatures at various locations within the catalyst bed are not observable in real-life circumstances. For example, in the case of a bimetallic catalyst, the bed temperature of 220 °C became 300 °C to 400 °C and subsequently to 450 °C with 3% hydrogen content as the methanol vapor went from 10% to 20% and 30%, respectively. This implies that the heat generated by burning methanol raises the bed temperature and improves the oxidation reaction's efficiency.

With air and 3% hydrogen, the bed temperature rises to 240 °C, which is sufficient to ignite methanol even after the hydrogen is switched off. A minimum concentration of 10% methanol further increases the bed temperature to 340 °C. Sequential co-feeding of VOCs can also participate in the catalytic combustion process. For example, adding a gaseous reactant mixture of air, 10% toluene, and 10% methanol vapor increases the bed temperature to 580 °C. Increasing 20% and 30% toluene vapors concentration further raises the bed temperature to 750 °C and 860 °C, respectively. This demonstrates that the exothermic combustion reaction happens and concludes in the upper section of the catalyst bed.

Both 10% methanol and VOCs' concentration similarly affect the VOCs' conversions and bed temperatures for benzene, ethyl benzene, and xylene. However, the bed temperature for benzene is higher than ethyl benzene and xylene, which have lower calorific values than benzene and toluene, resulting in relatively lower temperature increases. The catalytic active sites and reactants were heated on the spot by simply burning methanol

over a $PdPt/Al_2O_3$ catalyst. This catalyst serves both the H_2-ignited methanol and VOCs combustion. At normal temperatures, the fine PdPt particles in the spent $PdPt/Al_2O_3$ catalyst could begin the combustion of methanol and, at higher temperatures, complete the combustion of VOCs.

4. Experimental Section

4.1. Preparation of Catalyst

Both 1 wt% Pd/Al_2O_3 and $PdPt/Al_2O_3$ catalysts were prepared via the incipient wetness impregnation method, using alumina as the support. To achieve PdPt loading on alumina, equal molar amounts of 0.05 mol/L of each precursor in solution were used, consisting of 2.2 g of $PdCl_2$ and 6.5 g of $H_2PtCl_6 \cdot 6H_2O$ (both salts were purchased from CNMC Shenyang Research Institute of Nonferrous Metals Co., Ltd., Shenyang, China). The alumina support, consisting of spherical particles with diameters between 2 and 3 mm, was purchased from Dalian Bonuo Biochemical Reagent Company, Dalian China. The impregnated sample was dried at 120 °C for 8 h and then calcined at 500 °C for 5 h with a heating rate of 5 °C/min, and finally it was reduced in H_2 at 500 °C for 2 h with a flow rate of 300 mL/min.

4.2. Catalyst Characterizations

The specific surface areas of the fresh and spent catalysts were determined using the Brunauer–Emmett–Teller (BET) analysis method, employing N_2 adsorption at −196 °C with a Micromeritics ASAP 2460 instrument. X-ray diffraction (XRD) patterns were obtained using a PANalytical PW 3040/60 X'Pert PRO diffractometer equipped with a Cu K radiation source (λ = 1.5406 Å), operating at 40 kV and 40 mA. Transmission electron microscopy (TEM) and scanning transmission electron microscopy (STEM) were conducted on a JEOL JEM-2100F, Japan Electronics Co., Ltd. (Tokyo, Japan; Abingdon upon Thames, England) at 200 keV. Energy dispersive X-ray spectroscopy (EDS) analysis was carried out using an Oxford Instruments ISIS/INCA energy dispersive X-ray spectroscopy (EDS) system with an Oxford Pentafet Ultra-thin Window (UTW) Detector. Specimens for TEM and STEM analysis were prepared by depositing a suspension of the powdered sample on a lacey carbon-coated copper grid.

4.3. Reactor Setup and Performance Test

In the experimental setup, a fixed-bed reactor composed of a quartz tube with dimensions 10 mm inner diameter and 30 cm length was utilized. Within the reactor, 0.5 g of $PdPt/Al_2O_3$ catalyst (with a volume of 0.78 cm^3) was supported in the middle by a ceramic honeycomb (200 mesh). A k-type thermocouple was inserted into the catalyst bed for temperature measurement. The configuration of the packing is illustrated in Scheme 1. VOCs, including methanol and aromatic hydrocarbons such as benzene, toluene, ethylbenzene, and xylene, were simulated by bubbling chemical vapor obtained from respective sources (e.g., Fuyu chemicals-Tianjin Fuyu Fine Chemicals Co., Ltd.) through flowing air at rates of 100, 200, and 300 mL/min. This resulted in vapor concentrations of 10%, 20%, and 30%, with methanol fixed at 10% vapor concentration. Table 1 presents the nominal concentrations and calorific values for various VOCs–air mixtures.

Hydrogen was supplied from a high-purity hydrogen generator (Beijing Zhonghuipu, SPH-300A, Zhonghuipu Analytical Technology Research Institute, Beijing, China), and the flow rates of air and H_2 were controlled by calibrated mass flow controllers, maintaining a total flow rate of 1000 mL/min. This corresponded to a gas hourly space velocity of 120,000 mL/g-h or 77,000 h^{-1}. The reactants and products were analyzed using a mass spectrometer (Hiden Analytical, HPR-20, R&D, Beijing Ingelhead Analytical Technology Co., Ltd., Beijing, China), monitoring signals of H_2 (m/z = 2), methanol (m/z = 31), benzene (m/z = 78), toluene (m/z = 91), ethylbenzene (m/z = 91), xylene (m/z = 91), and CO_2 (m/z = 44). Temperature-programmed catalytic reaction experiments were conducted

to determine light-off temperatures using an electric heating furnace at a ramp rate of 5 °C/min from room temperature to 750 °C.

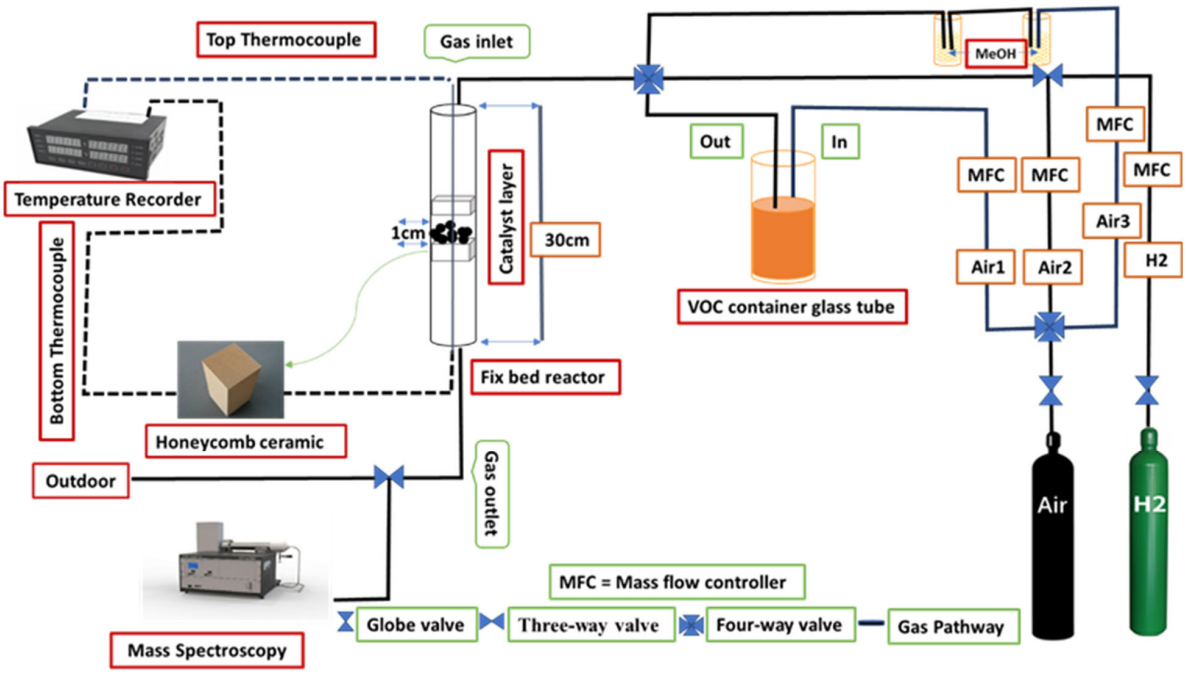

Scheme 1. Diagram of experimental device of hydrogen-ignited-methanol catalytic combustion.

5. Conclusions

In this study, significant insights have been gained into catalysis and redress for the environment. For the treatment of VOCs, thorough experimentation and analysis have demonstrated that a bimetallic catalyst can enhance catalytic activity via the combustion of methanol ignited by hydrogen. In this study, 1% Pd/Al_2O_3 and $PdPt/Al_2O_3$ catalyst were prepared, and their activity was evaluated in the hydrogen-ignited-methanol catalytic oxidation of VOCs, specifically benzene, toluene, ethyl-benzene, and xylene. The study observed varying temperatures in the catalytic combustion of these VOCs compounds under similar reaction conditions. Benzene exhibited the highest temperature at the lowest VOCs concentration, while toluene, with a high VOCs quantity, reached a temperature of 900 °C. Ethyl benzene, containing a substantial quantity of VOCs, showed a maximum bed temperature of 600 °C. In contrast, xylene displayed the lowest bed temperature among these VOCs. One noteworthy observation was hydrogen's role in initiating the methanol combustion process and that the synergy with the bimetallic catalyst contributed to a more rapid and controlled reaction, leading to the effective elimination of VOCs. This dual-action mechanism highlights the potential for optimizing catalytic systems by considering multiple variables, offering a pathway for future research endeavors. The research demonstrated the enhanced catalytic activity of the bimetallic catalyst during methanol catalytic combustion, showcasing improved efficiency and reactivity compared to traditional combustion. The persistent performance of spent catalysts offers cost-effective and sustainable industrial applications, underlining the need to study catalyst lifetime for greener industrial processes.

Supplementary Materials: The following supporting information can be downloaded at https://www.mdpi.com/article/10.3390/catal14090637/s1, Figure S1: The SEM images of mesoporous alumina support, Figure S2: VOCs' conversion curves and the corresponding catalyst bed temperature profiles of various VOCs with co-combustion of +10 MeOH started with 3%H_2 ignition over 0.5 g $PdPt/Al_2O_3$ catalyst, Figure S3: MeOH conversion curves and the corresponding catalyst bed temperature profiles of various VOCs with co-combustion of +10 MeOH started with 3%H_2 ignition over 0.5 g $PdPt/Al_2O_3$ catalyst. The SEM images of mesoporous alumina support.

Author Contributions: S.M. and L.U. synthesized the catalysts, performed most of the experiments, and collected and analyzed the data. L.C. and J.-C.Z. established the reaction setup and validated the concept. P.R.M. paper revision. W.-Z.L. designed the study and supervised the project. All authors contributed to the general discussion and co-wrote the manuscript. All authors have read and agreed to the published version of the manuscript.

Funding: This work was supported by the "Transformational Technologies for Clean Energy and Demonstration", Strategic Priority Research Program of the Chinese Academy of Sciences, (XDA21040200).

Data Availability Statement: Data presented in this article are available either in the main manuscript or upon reasonable request from the corresponding author.

Conflicts of Interest: The authors declare no conflicts of interest.

References

1. Fang, Y.; Yang, J.; Pan, C. The Surface/Interface Modulation of Platinum Group Metal (PGM)-Free Catalysts for VOCs and CO Catalytic Oxidation. *ACS Appl. Mater. Interfaces* **2024**, *16*, 37379–37389. [CrossRef]
2. Wang, L.; Zhang, C.; He, H.; Liu, F.; Wang, C. Effect of Doping Metals on OMS-2/γ-Al_2O_3 Catalysts for Plasma-Catalytic Removal of o-Xylene. *J. Phys. Chem. C* **2016**, *120*, 6136–6144. [CrossRef]
3. Huang, S.; Zhang, C.; He, H. Complete oxidation of o-xylene over Pd/Al_2O_3 catalyst at low temperature. *Catal. Today* **2008**, *139*, 15–23. [CrossRef]
4. Ren, Y.; Lei, X.; Wang, H.; Xiao, J.; Qu, Z. Enhanced Catalytic Performance of La-Doped CoMn2O4 Catalysts by Regulating Oxygen Species Activity for VOCs Oxidation. *ACS Catal.* **2023**, *13*, 8293–8306. [CrossRef]
5. Gil-Barbarin, A.; Gutiérrez-Ortiz, J.I.; López-Fonseca, R.; de Rivas, B. Promotion of Cobalt Oxide Catalysts by Acid-Etching and Ruthenium Incorporation for Chlorinated VOC Oxidation. *Ind. Eng. Chem. Res.* **2024**, *63*, 3003–3017. [CrossRef]
6. Shan, C.; Wang, Y.; Li, J.; Zhao, Q.; Han, R.; Liu, C.; Liu, Q. Recent Advances of VOCs Catalytic Oxidation over Spinel Oxides: Catalyst Design and Reaction Mechanism. *Environ. Sci. Technol.* **2023**, *57*, 9495–9514. [CrossRef]
7. Zha, K.; Wu, S.; Zheng, Z.; Huang, Z.; Xu, H.; Shen, W. Insights into Boosting SO_2 Tolerance for Catalytic Oxidation of Propane over Fe_2O_3-Promoted Co_3O_4/Halloysite Catalysts. *Ind. Eng. Chem. Res.* **2022**, *61*, 12482–12492. [CrossRef]
8. Sun, N.; Wang, L.; Zhang, Y.; Cao, Z.; Sun, J. $Co_2Cu_1Ce_yO_x$ Mixed Metal Oxide Nanoparticles with Oxygen Vacancies as Catalysts for Toluene Oxidation. *ACS Appl. Nano Mater.* **2023**, *6*, 18823–18836. [CrossRef]
9. Wu, P.; Zhao, S.; Yu, J.; Jin, X.; Ye, D.; Yang, S.; Qiu, Y. Effect of Absorbed Sulfate Poisoning on the Performance of Catalytic Oxidation of VOCs over MnO_2. *ACS Appl. Mater. Interfaces* **2020**, *12*, 50566–50572. [CrossRef]
10. Žumbar, T.; Arčon, I.; Djinović, P.; Aquilanti, G.; Žerjav, G.; Pintar, A.; Ristić, A.; Dražić, G.; Volavšek, J.; Mali, G.; et al. Winning Combination of Cu and Fe Oxide Clusters with an Alumina Support for Low-Temperature Catalytic Oxidation of Volatile Organic Compounds. *ACS Appl. Mater. Interfaces* **2023**, *15*, 28747–28762. [CrossRef]
11. Obraztsov, N.V.; Subbotin, D.I.; Pavlova, E.A.; Frolov, V.Y.; Belyaev, V.L. Synthesis of the nickel-containing catalyst on the aluminum oxide supporter produced by glycine-nitrate synthesis. *Mater. Today Proc.* **2020**, *30*, 528–531. [CrossRef]
12. Žumbar, T.; Ristić, A.; Dražić, G.; Lazarova, H.; Volavšek, J.; Pintar, A.; Zabukovec Logar, N.; Tušar, N.N. Influence of Alumina Precursor Properties on Cu-Fe Alumina Supported Catalysts for Total Toluene Oxidation as a Model Volatile Organic Air Pollutant. *Catalysts* **2021**, *11*, 252. [CrossRef]
13. Li, A.; Wang, P.; Yi, J.; Farhan, S.M.; Zhang, L.; Zhao, L.; Lei, L. Influence of M-Doped (M = Ba, Zr, La, and Ce) for Enhanced CO and C3H6 Catalytic Oxidation over Pd/Al_2O_3 Catalysts. *J. Phys. Chem. C* **2024**, *128*, 14638–14648. [CrossRef]
14. Abbasi, Z.; Haghighi, M.; Fatehifar, E.; Saedy, S. Synthesis and physicochemical characterizations of nanostructured Pt/Al_2O_3–CeO_2 catalysts for total oxidation of VOCs. *J. Hazard. Mater.* **2011**, *186*, 1445–1454. [CrossRef]
15. Chen, Z.; Li, J.; Yang, P.; Cheng, Z.; Li, J.; Zuo, S. Ce-modified mesoporous N_3-Al_2O_3 supported Pd-Pt nanoparticle catalysts and their structure-function relationship in complete benzene oxidation. *Chem. Eng. J.* **2019**, *356*, 255–261. [CrossRef]
16. Fu, X.; Liu, Y.; Yao, W.; Wu, Z. One-step synthesis of bimetallic Pt-Pd/MCM-41 mesoporous materials with superior catalytic performance for toluene oxidation. *Catal. Commun.* **2016**, *83*, 22–26. [CrossRef]
17. Maione, A.; Andre, F.; Ruiz, P. Structured bimetallic Pd-Pt/γ-Al_2O_3 catalysts on FeCrAlloy fibers for total combustion of methane. *Appl. Catal. B Environ.* **2007**, *75*, 59–70. [CrossRef]
18. Kim, S.C.; Park, Y.-K.; Nah, J.W. Property of a highly active bimetallic catalyst based on a supported manganese oxide for the complete oxidation of toluene. *Powder Technol.* **2014**, *266*, 292–298. [CrossRef]
19. Fan, X.; Wang, F.; Zhu, T.; He, H. Effects of Ce on catalytic combustion of methane over Pd-Pt/Al_2O_3 catalyst. *J. Environ. Sci.* **2012**, *24*, 507–511. [CrossRef]
20. Sultana, S.; Vandenbroucke, A.; Leys, C.; De Geyter, N.; Morent, R. Abatement of VOCs with Alternate Adsorption and Plasma-Assisted Regeneration: A Review. *Catalysts* **2015**, *5*, 718–746. [CrossRef]
21. Zhong, B.-j.; Yang, F. Characteristics of hydrogen-assisted catalytic ignition of n-butane/air mixtures. *Int. J. Hydrogen Energy* **2012**, *37*, 8716–8723. [CrossRef]

22. Zhong, B.-J.; Yang, Q.-T.; Yang, F. Hydrogen-assisted catalytic ignition characteristics of different fuels. *Combust. Flame* **2010**, *157*, 2005–2007. [CrossRef]
23. Jiang, Y.; Chen, Y.; Wang, R.; Lu, W.; Liu, W.; Zhang, Y. Investigation on the effects of blending hydrogen-rich gas in the spark-ignition engine. *Energy Rep.* **2022**, *8*, 797–803. [CrossRef]
24. Verhelst, S.; Turner, J.W.G.; Sileghem, L.; Vancoillie, J. Methanol as a fuel for internal combustion engines. *Prog. Energy Combust. Sci.* **2019**, *70*, 43–88. [CrossRef]
25. Jang, E.J.; Lee, J.; Oh, D.G.; Kwak, J.H. CH4 oxidation activity in pd and Pt–Pd bimetallic catalysts: Correlation with surface PdO x quantified from the DRIFTS study. *ACS Catal.* **2021**, *11*, 5894–5905. [CrossRef]
26. Ho, P.H.; Shao, J.; Yao, D.; Ilmasani, R.F.; Salam, M.A.; Creaser, D.; Olsson, L. The effect of Pt/Pd ratio on the oxidation activity and resistance to sulfur poisoning for Pt-Pd/BEA diesel oxidation catalysts with high siliceous content. *J. Environ. Chem. Eng.* **2022**, *10*, 108217. [CrossRef]
27. Kim, S.-I.; Im, M.; Cho, E.; Jang, H.; Jang, S.Y.; Kim, D.W.; Kim, K.W.; Heo, I.; Kim, Y.J.; Lee, J.H. Effects of thermal aging on the electronic and structural properties of Pt-Pd and toluene oxidation activity. *Sci. Total Environ.* **2022**, *847*, 157482. [CrossRef]
28. Wu, P.; Cao, Y.; Zhao, L.; Wang, Y.; He, Z.; Xing, W.; Bai, P.; Mintova, S.; Yan, Z. Formation of PdO on Au–Pd bimetallic catalysts and the effect on benzyl alcohol oxidation. *J. Catal.* **2019**, *375*, 32–43. [CrossRef]
29. Ho, P.H.; Woo, J.W.; Feizie Ilmasani, R.; Han, J.; Olsson, L. The role of Pd–Pt interactions in the oxidation and sulfur resistance of bimetallic Pd–Pt/γ-Al_2O_3 diesel oxidation catalysts. *Ind. Eng. Chem. Res.* **2021**, *60*, 6596–6612. [CrossRef]
30. Mussio, A.; Danielis, M.; Divins, N.r.J.; Llorca, J.; Colussi, S.; Trovarelli, A. Structural evolution of bimetallic PtPd/CeO_2 methane oxidation catalysts prepared by dry milling. *ACS Appl. Mater. Interfaces* **2021**, *13*, 31614–31623. [CrossRef]
31. Narui, K.; Yata, H.; Furuta, K.; Nishida, A.; Kohtoku, Y.; Matsuzaki, T. Effects of addition of Pt to PdO/Al_2O_3 catalyst on catalytic activity for methane combustion and TEM observations of supported particles. *Appl. Catal. A Gen.* **1999**, *179*, 165–173. [CrossRef]
32. Song, M.; Zeng, W.; Li, L.; Wu, X.; Li, G.; Hu, C. Effect of the Zr/Al Molar Ratio on the Performance of Cu/ZrO_2–Al_2O_3 Catalysts for Methanol Steam Reforming. *Ind. Eng. Chem. Res.* **2023**, *62*, 3898–3908. [CrossRef]
33. Yang, X.; Ma, X.; Yu, X.; Ge, M. Exploration of strong metal-support interaction in zirconia supported catalysts for toluene oxidation. *Appl. Catal. B Environ.* **2020**, *263*, 118355. [CrossRef]
34. Chen, K.; Wan, J.; Wang, T.; Sun, Q.; Zhou, R. Construction of bimetallic Pt–Pd/CeO_2–ZrO_2–La_2O_3 catalysts with different Pt/Pd ratios and its structure–activity correlations for three-way catalytic performance. *J. Rare Earths* **2023**, *41*, 896–904. [CrossRef]
35. Kozhukhova, A.; Du Preez, S.; Shuro, I.; Bessarabov, D. Development of a low purity aluminum alloy (Al6082) anodization process and its application as a platinum-based catalyst in catalytic hydrogen combustion. *Surf. Coat. Technol.* **2020**, *404*, 126483. [CrossRef]
36. Schefer, R.; Robben, F.; Cheng, R. Catalyzed combustion of H_2/air mixtures in a flat-plate boundary layer: I. Experimental results. *Combust. Flame* **1980**, *38*, 51–63. [CrossRef]
37. Ullah, L.; Munsif, S.; Cao, L.; Zhang, J.-C.; Li, W.-Z. Facile Abatement of Oxygenated Volatile Organic Compounds via Hydrogen Co-Combustion over Pd/Al_2O_3 Catalyst as Onsite Heating Source. *Catalysts* **2024**, *14*, 372. [CrossRef]
38. Saint-Just, J.; Der Kinderen, J. Catalytic combustion: From reaction mechanism to commercial applications. *Catal. Today* **1996**, *29*, 387–395. [CrossRef]